Practical Experience in using a Topological Model of a Core-Type Three-Phase Transformer – No-Load and Inrush Conditions

S. E. Zirka, Y. I. Moroz, H. Kr. Høidalen, A. Lotfi, N. Chiesa, and C. M. Arturi

***Abstract*—This paper describes an experience in transformer modeling based on open-circuit test data obtained for a wide range of terminal voltages and inrush current measurements that were carried out for different residual fluxes of a 300 kVA transformer. The core type transformer model is based on a dynamic hysteresis model which is employed individually in the legs and yokes. We start with the case where the core geometry and winding turns are known when fitting the model. The method proposed is then extended to the case where only the nameplate data and the measured no-load losses and currents are available. For this latter case, an optimization model fitting is developed.**

***Keywords*: Transformers, hysteresis, test report, residual flux, inrush current, optimization fitting.**

I. Introduction

TOPOLOGICAL transformer models are now widely used because they reproduce phase-to-phase magnetic coupling as well as different operation conditions of the legs and yokes in saturation. The latter is achieved by shunting each branch of the core model with reluctances that represent magnetic flux paths in the non-ferromagnetic environment [1].

An important initial stage in developing transformer model is the fit of its parameters to short circuit (SC) and open circuit (OC) test data. While the calculation of the SC parameters is relatively straightforward, there were obvious difficulties in fitting the model to no-load losses P_0 and currents I_0 measured for a wide range of terminal voltage V [2]. The rapid increase of the measured dependencies $P_0(V)$ and $I_0(V)$ at voltages exceeding 1.05-1.10 pu indicates that the core approaches saturation. This means that the accurate model tuning at elevated voltages is also important for subsequent simulations of inrush current events, which are characterized by heavy saturated core branches.

To make the model applicable to a range of low-frequency transients [3], the core branches should be hysteretic and frequency dependent. Their analysis is complicated by the need to account for the core geometry, in which the legs and yokes are represented individually, but are modeled simultaneously when analyzing the transformer performance. The difficulties encountered in building such topological models compel many authors to join the legs and yokes of the model into composite solid branches and to use *static* hysteresis elements mistakenly called *dynamic* models. A typical example is the "semi-topological" model [4] and some models referred to in [4] and [3].

Comprehensive reviews of transient transformer models can be found in [2], [5], [6], and [7]. Typically, transformer modeling is complicated by the lack of knowledge about the core material. Even if the core steel is specified by manufacturer, the actual characteristics of the core branches are always different from those expected from catalog data [8]. It is practically impossible to extract all necessary information about the core branches from flux linkages, λ, and currents, i, measured on winding terminals. As seen in Fig. 1, the λ–i curves measured on the wye-connected windings of a three-legged core transformer considered in this paper are quite different, and thus have a limited value.

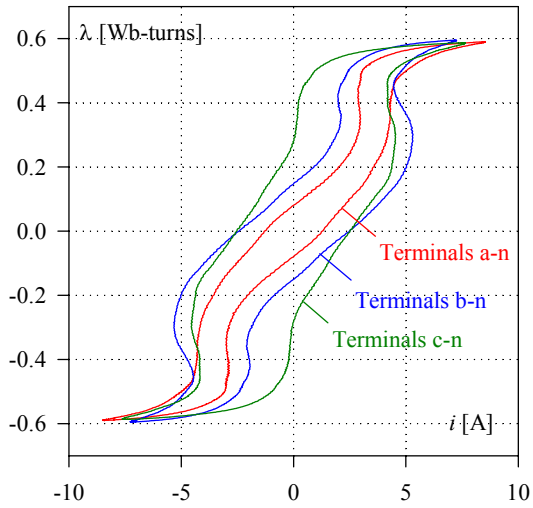

Fig. 1. Terminal hysteresis loops measured on the LV side of 300 kVA Y-yn transformer at V = 97.5% (HV windings are open-circuit in the test).

The ingenious methods of measuring individual λ–i curves of the core branches [7], [9] require dedicated experiments and yield *dynamic* (50-60 Hz) hysteresis loops. To make

This work was financial supported from the EM-Transients project at SINTEF Energy Research and the Norwegian Research Council.

S. E. Zirka and Y. I. Moroz are with the Dnipro National University, Dnipro, Ukraine 49050 (zirka@email.dp.ua).

H. Kr. Høidalen and A. Lotfi are with the Norwegian University of Science and Technology, N-7491 Trondheim, Norway (hans.hoidalen@elkraft.ntnu.no).

N. Chiesa is with Statoil, Norway (NChie@statoil.com).

C. M. Arturi is with the Politecnico di Milano, Milan 20133, Italy (cesaremario.arturi@polimi.it).

transformer model frequency-sensitive and to be able to predict residual fluxes [10], *static* hysteresis loops of the core material should also be reasonably guessed. So predicting *static* loops is another task, which is common for both single- and three-phase transformers.

These difficulties in the core characterization make the transformer modeling heuristic regarding the choice of the core material and suggest to start with catalog data of most probable grain-oriented (GO) steels. This approach is also justified by the fact that test reports seldom include data for excitations exceeding 110% while steel manufacturers typically provide *B-H* curves reaching 2 T which corresponds to the voltage of approximately 120%. The latter is particularly important to reproduce the model behavior at highest voltages when the magnetization current is very sensitive to the excitation. We draw attention to this model feature because, concentrating on the accuracy of the "last-segment slope", that is the incremental saturation inductance, the saturation *level* of the magnetization curve is often left without proper care, as for example in [11].

The flexibility of the transformer model developed is ensured by using a modified dynamic hysteresis model (DHM) which is employed in dedicated Fortran codes and has been recently implemented into ATPDraw [3]. This model implementation is based on steel manufacturer's data including static hysteresis loops, catalog losses, and DC magnetization curves reaching high flux densities.

The model fitting in Sections II to VII is carried out for a transformer with known design parameters. In Section VIII, an optimization model fitting is developed for the case when the core and winding parameters are unknown.

II. Transformer and Test Data

A test object for this study is a 300 kVA, 11.43/0.235 kV, 50 Hz, Yyn distribution transformer described in details in [2], [11], and [12]. Its short circuit voltage and power loss are $V_{SC} = 4.1\%$ and $P_{SC} = 3.187$ kW. The 3-legged core was assembled, *presumably*, from the Armco 0.3-mm thick steel M5 with resistivity of 0.48 μΩ·m. Cross sections of the legs (0.017528 m^2) and yokes (0.019812 m^2) were determined from geometrical dimensions of their packs. The actual cross sections are calculated by multiplying these values by the stacking factor of the core, S_F, which is one of the model variables in Sections V and VIII.

Some data from OC test report are given in Table I. In accordance with the standards [13], [14] the true rms voltages V_{rms} and the average-absolute (rms-scaled) voltages V_{avg} were measured simultaneously across the low voltage (LV) terminals. Table I also contains total harmonic distortions (THD) of the LV voltages calculated from the voltage waveforms recorded during the OC test.

The rapidly increasing THD as well as the increasing difference between V_{rms} and V_{avg} at $V_{avg} > 100\%$ evidences substantially nonsinusoidal voltages at high excitations (several voltage waveforms of phase B are shown in Fig. 2). This means that the modeling of the OC regime using the sinusoidal voltages with V_{rms} in Table I may be completely wrong at high excitations. For example, the use of sinusoidal voltage with $V_{rms} = 127.73\%$ and $S_F = 0.95$ results in the peak flux density $B_m = 2.223$ T, which is much higher than the "technical saturation" of any GO steel (2.02-2.05 T). So the use of the true rms voltages (V_{rms}) can drive the modeled core into a false saturation that makes the model fitting impossible.

In this situation, the following two alternative methods are the use of the recorded voltage waveforms and the calculations using sinusoidal voltages with the average (rms-scaled) voltages V_{avg}. The use of the voltage waveforms is complicated by the difficulties in the model initialization at multi-harmonic excitations. So the modeling is first carried out using the average voltages V_{avg} and then verification of the calculated results is carried out using the voltage waveforms.

TABLE I. Transformer Open Circuit Test Report

OC test	V_{rms},%	V_{avg},%	THD,%	I_0,%	P_0, kW
	64.17	64.09	0.82	0.163	0.215
Voltage	80.80	80.55	1.48	0.275	0.353
on LV	97.52	96.67	3.26	0.600	0.563
side	101.54	100.24	4.64	0.780	0.635
	105.33	103.35	6.75	1.061	0.714
	108.91	105.99	9.52	1.493	0.794
	113.09	108.83	13.13	2.321	0.892
	116.46	111.03	15.86	3.403	0.979
	118.41	112.28	17.26	4.270	1.036
	120.59	113.60	18.79	5.545	1.109
	125.44	116.01	22.55	10.409	1.341
	127.73	116.79	24.57	15.261	1.556

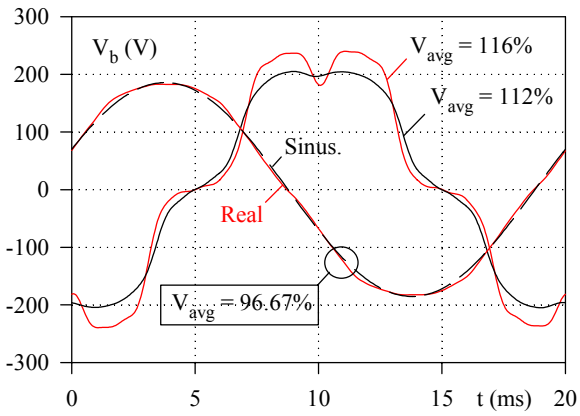

Fig. 2. Phase voltage waveforms on the LV terminals.

III. Transformer Models

The topological magnetic circuit of the transformer considered is shown in Fig. 3. If switches *S* are open, the scheme is similar to that in [6]. The MMFs F_L and F_H represent the LV and HV windings respectively. The magnetic flux paths in the core are shown as solid rectangles, which represent the legs (elements R_a, R_b, R_c) and yokes (R_{ab} and R_{bc}). All these core branches are described using the DHM considered in Section IV.

The off-core flux paths are characterized by linear reluctances shown by unshaded rectangles: R_{01} for paths between the inner (LV) windings and the core legs, R_{12} for paths in the

equivalent leakage channels between the LV and HV windings, R_{03} for paths beyond the windings (from yoke to yoke), and R_{04} for fringing flux paths, which come into play when the yokes approach saturation. Reluctances R_g take into account the air gaps Δ in the core joints. They are related to the legs of cross section S_{leg} and are calculated as $\Delta/(\mu_0 S_{leg})$ where the value of Δ (6 μm) will be determined in Section VI.

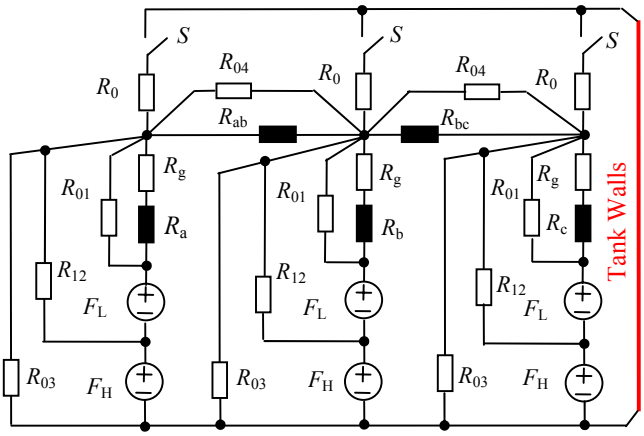

Fig. 3. Magnetic circuit of the two windings three-legged core transformer. To model the tank walls, magnetic switches *S* should be closed.

When switches *S* in Fig. 3 are closed, reluctances R_0 characterize the flux paths from the core to the tank walls. So, these reluctances also account *indirectly* for the influence of the cover and bottom of the tank. A good illustration of the zero-sequence flux paths in the transformer considered is Fig. 3 in [15] which shows that the most loaded part of the tank is a central belt of the tank walls.

By using the principle of duality, the reluctive magnetic circuit in Fig. 3 is transformed into its inductive equivalent shown between the ideal transformers in Fig. 4. The linear inductances *L* in Fig. 4 are indexed with the same symbols as the linear reluctances *R* in Fig. 3; their values are linked by the relationship $L = N_1^2 / R$ where N_1 is the number of turn in the LV winding. The five DHM-elements are ATPDraw implementations of the DHM which reproduce the core legs and yokes. The ladder (Cauer) circuit in Fig. 4 represents the central belt of the thick tank walls [16].

According to [12], the leakage inductance L_{12} = 23.2 μH. The channels between the core and the inner (LV) windings are characterized by inductance $L_{01} = K\ L_{12}$ [6], where the coefficient *K* is a fitting parameter influencing inrush current peaks. It will be found in Section VI-A that $K = 0.62$.

The open switches *S* in the magnetic circuit (Fig. 3) correspond to the closed switches *S* in the electric circuit of Fig. 4. In this *simplified* scheme, the value of inductances L_{03} is set equal to 0.42 mH as specified in [12]. Inductances L_{03} and L_0 in the *full* model (the model with Cauer circuit) are found in Section VI-B. The invariable fringing inductances, L_{04} = 0.018 mH, were chosen in accordance with the method in [16].

In modeling the no-load test from the LV terminals as well as in the initial modeling of inrush currents on the HV side, we shall use the *simplified model* with the closed switches *S* in Fig. 4 (they isolate the wall sub-model [16] from the remaining model). The influence of the tank walls on the inrush currents will be considered in Section VI-B.

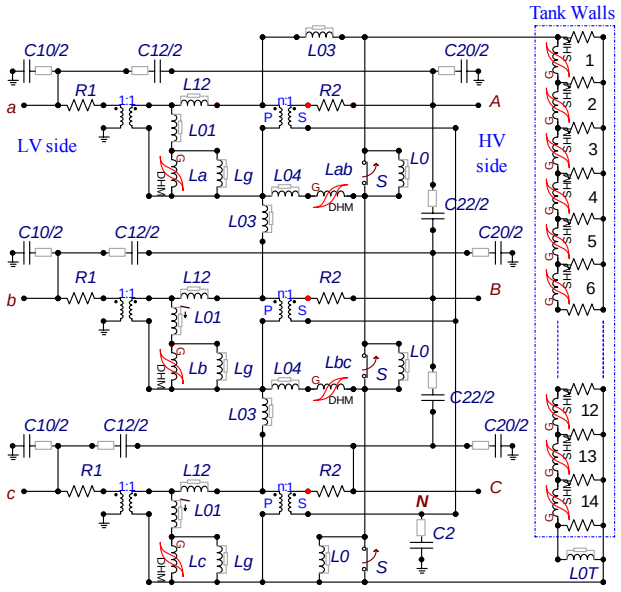

Fig. 4. Electric model of the transformer. To model tank walls as a virtual winding with eddy currents, switches *S* should be open by duality.

Inductances L_g take into account the air gaps in the core, and control the residual flux in the legs. Resistors R_1 and R_2 represent the resistances of the LV and HV windings. Six ideal transformers serve to relate the model parameters to the number of turns N_1.

In addition to the inductive and resistive elements of the model, the measured capacitances (given in [12]) are added to the scheme in Fig. 4. All winding capacitances have been divided into two equal parts and connected to (and between) corresponding terminals of the HV and LV windings. Since the LV neutral is earthed and HV neutral *N* is isolated, the second halves of the capacitances C_{10}, C_{12}, and C_{20} are collected into a single capacitance C_2 between the neutral *N* and earth.

IV. Dynamic Hysteresis Model

The three-component hysteresis model used in the study consists of a rate-independent (static) hysteresis inductor and two resistive elements, linear and nonlinear, reproducing classical eddy-current and excess losses respectively.

The hysteresis inductor is an ATP implementation [17] of an inverse static hysteretic model (SHM), which transforms $H_h(B)$ curves into $i(\lambda)$ dependencies. Its input is the flux density *B* (or flux linkage λ), and the output is the magnetic field strength H_h (or current *i*).

The classical and excess fields (and hence losses) are reproduced by the bracketed terms in the DHM (1) multiplied by the loss coefficient K_{loss}:

$$H(t) = H_h(B(t)) + K_{loss}\left(k_{ec}\frac{dB}{dt} + g(B)\left|\frac{dB}{dt}\right|^{0.5}\delta \right). \qquad (1)$$

Here the constant $k_{ec} = d^2/(12\rho)$ is determined by the lamination thickness d and the resistivity ρ of the core material, and $\delta = \pm 1$ is the sign of the derivative dB/dt.

The advantage of the DHM (1) over the existing DHMs or the simplest core models with a parallel-connected SHM and a constant loss resistor, is caused by the function $g(B)$ in the excess-field term in (1). The key feature of this function is its increase with $|B|$, which is especially pronounced when approaching saturation. The rise of $g(B)$ and thus $H(t)$ results in a widening of the dynamic hysteresis loops and increases specific losses of the core material at high flux densities (see Figs. 8 and 9 of [3]).

As no dynamic loops are usually provided by catalogs, we were oriented to the function $g(B)$ adjusted to GO steel measured in [18], and scaled it to the catalog loss data. Several typical steels (M4, M5, H1) can be chosen from the material list of the DHM [19].

Although the DHM has shown performance in agreement with Epstein frame measurements, the model should always be fitted to the no-load loss of a specific transformer. This is because the real core loss is usually greater than that expected from steel catalog data or Epstein tests [8]. The loss adjustment of the DHM employed is carried out by multiplying the two last terms in (1) by the loss coefficient K_{loss}, which is the only fitting parameter of the DHM after the electrical steel has been chosen from the model list. Each item of the list contains parameters of the SHM and a pointwise saturation curve $H(B)$. The tangent of its final segment is equal to μ_0, and the last point is at the level of the so-called *technical saturation* (2.03-2.05 T), which is typical of the majority of transformer (GO) steels.

The rest of fitting parameters are related to the transformer, but not to the DHM. The main of these is the stacking factor (S_F) of the core and the air gaps Δ at the core joints. Their influence is considered in Section V and VI.

V. The Fitting of the DHM-Based Transformer Model

The fitting of the DHM within the transformer model is carried out using both the no-load test report in Table I (measured from the LV side) and inrush current data obtained from the HV side.

A. The fitting to the no-load test report using catalog data of GO steel Armco M5

When modeling transformer supplied from a variac on the LV side (HV winding is open), the coefficient K_{loss} and the stacking factor S_F are first adjusted. The need for changing these coefficients from their initial unit values is shown in Fig. 5 where the no-load transformer losses and currents calculated with $K_{loss} = 1$ and $S_F = 1$ are obviously less than measured.

An increase of K_{loss} increases the losses (see curve 2 in Fig. 5(a)), but does not influence the currents (curve 2 in Fig. 5(b) coincides with curve 1). The effect of decreasing S_F (from 1 to 0.965) is negligible at small voltages, but quickly increases at $V_{avg} > 100\%$ (see curves 3 in Fig. 5).

The influence of S_F is maximum at the highest voltage ($V_{avg} = 116.79\%$), when flux densities in the legs reach 1.998 – 1.999 T, that is close to the technical saturation. At these induction levels, the magnetization current is highly sensitive to the voltage (at a fixed S_F) or to S_F (at the fixed voltage). So, even the smallest decrease in S_F (the decrease in the effective cross section of the legs) leads to a drastic rise of the current drawn from the source. Fig. 5(a) also shows that passing from $S_F = 1$ (curve 2) to $S_F = 0.965$ (curve 3) increases the no-load losses (again, at high voltages). This is mainly explained by the fast rise of the specific loss in any GO steel at $B_m > 1.9$ T. Besides, the losses in the LV winding are not negligible at the highest voltages.

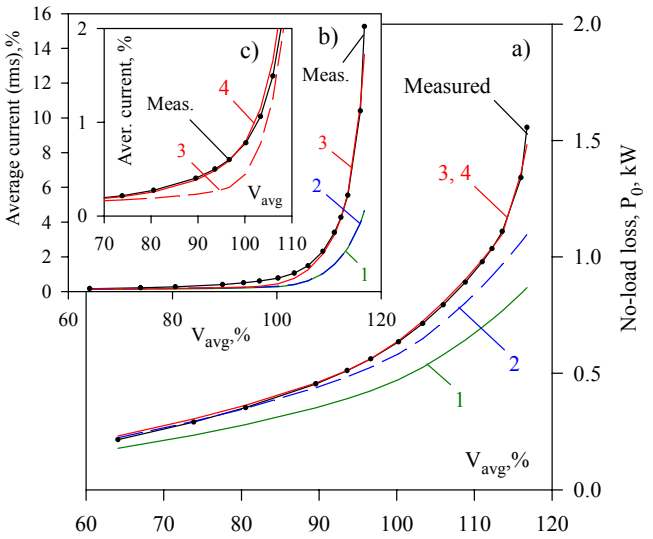

Fig. 5. The influence of the coefficient K_{loss} and stacking factor (S_F) on the calculated no-load currents and losses. Curves 1: $K_{loss} = 1$ and $S_F = 1$; curves 2: $K_{loss} = 1.3335$ and $S_F = 1$; curves 3: $K_{loss} = 1.3335$ and $S_F = 0.965$. Curves 4 were obtained with the skewed hysteresis loop.

B. Correction of the no-load current using skewed hysteresis loop

It is noted that the transformer model reproduces no-load losses perfectly, but the currents calculated around the *rated* voltage are markedly lower than measured (see curve 3 in Fig. 5(c), which is a magnification of a lower part of Fig. 5(b)). This imperfection cannot be corrected by changing K_{loss} or S_F without introducing noticeable distortions in the model operation at low and high voltages.

This suggests the idea [12] to improve the transformer model by accounting for the impact of the corners and T-joint areas of the core where the magnetic fluxes in the core laminations deviate from the rolling direction.

To implement this idea, it can be noted that static hysteresis loops, provided by a catalog, should be considered only a first approximation to the actual B-H or λ-i characteristics of the core branches. The major reason is the influence of the core joints where magnetization is changing in all three directions, rolling (RD), transverse (TD), and normal (ND). The latter is necessitated by the need of the flux to bypass the butt-to-butt air gaps in the overlap-joint region.

Following Bozorth (Fig.11-2 in [20]), we may represent magnetization curves of GO steel in large (kA/m) fields as

shown schematically in Fig. 6.

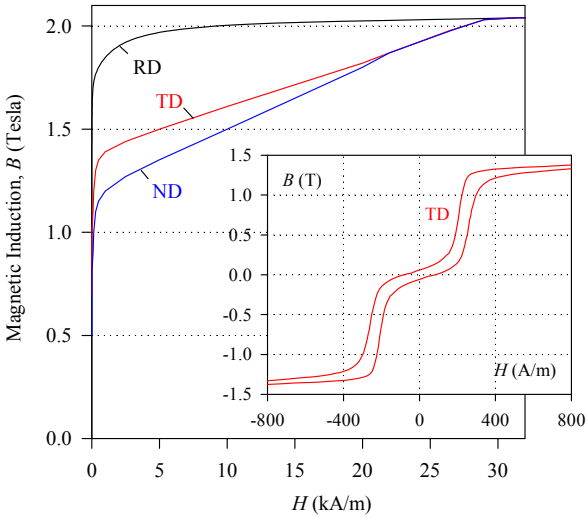

Fig. 6. Magnetization curves of GO steel in rolling, transverse, and normal directions. The TD loop in the insert is taken from [21].

Now, we can recall that the hysteresis loop of a core branch (leg or yoke) is its averaged (homogenized) model, which represents the processes in all parts of the branch implicitly. The whole core branch can be approximately divided into two segments (regions). The steel of the long central segment 1 is magnetized along the RD, while in the corners and T-joints (they form segment 2), the flux deviates from the RD (easy magnetization direction) and passes in the TD and ND, which are much harder for the magnetization [22].

It is seen in Fig. 6 that curves TD and ND deviate sharply from curve RD at $B > (1.2–1.3)$ T when a saturation tendency appears in the TD and ND curves (the inset of Fig. 6 shows the static loop measured in the TD [21]). It should be noted, however, that the "saturation" seen in this loop is an intermediate stage, and the final saturation level is the same for all three curves in Fig. 6. To recalculate these curves into a single representative curve of the branch, we can note that segments 1 and 2 are connected in series and that the segment 2 is about an order of magnitude shorter than segment 1. This means that the catalog hysteresis loop should be skewed only in its *upper* part to obtain equivalent loop of the core branch.

The skewed loop $H(B)$ in Fig. 7 was obtained from the catalog (RD) loop $H_{cat}(B)$ of steel M5 using the expression

$$H(B) = H_{cat}(B) + 4\,B^7. \qquad (2)$$

The odd power of the induction B in (2) ensures the central symmetry of the skewed loop with respect to the origin. The multiplier 4 in this formula was chosen so as to reproduce the no-load current as shown by curve 4 in Fig. 5(c). It is important that the skewing of the catalog loop has no visible impact on the no-load losses, see Fig. 5(a).

C. *The model fitting under the real terminal voltages*

In the previous modeling, the nonsinusoidal terminal voltages like those in Fig. 2 were replaced by sinusoidal voltages with corresponding V_{avg}. To evaluate the acceptability of such a replacement, all terminal voltages were expanded into Fourier series. It was found in numerical experiments that 21 harmonics are sufficient to represent accurately the most distorted voltage.

The calculations with the Fourier-expanded voltages were carried out using a dedicated Fortran program, in which a Gear integration method is used for solving a system of nonlinear differential equations describing the transients in the original *magnetic* circuit. The first reason for using the Fortran model is its cross-checking with the ATP model, which solves the duality-derived *electrical* circuit for node voltages and uses trapezoidal integration.

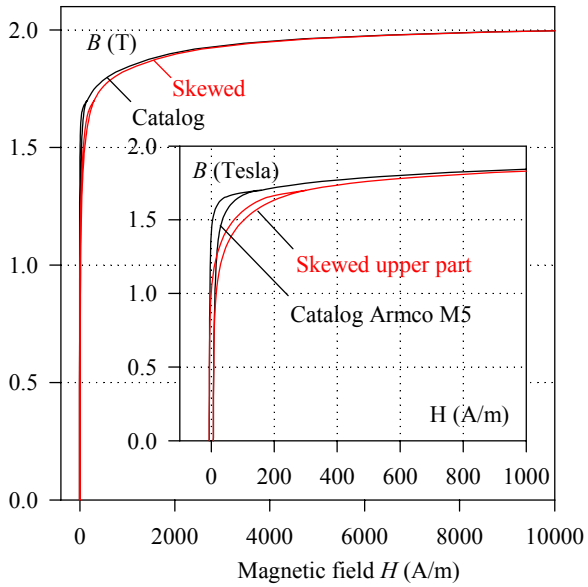

Fig. 7. Catalog and skewed loops of Armco steel M5.

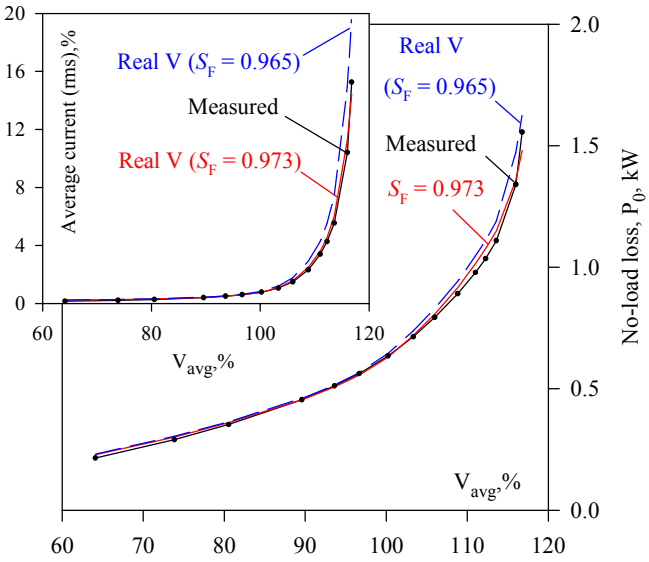

Fig. 8. No-load losses and currents calculated for real voltages with S_F = 0.965 and S_F = 0.973.

The second and the main reason of using the Fortran model is the difficulties in obtaining symmetrical flux densities in all the core branches after the auto-initialization of any model at multi-harmonic excitations. This problem is usually overcome

by using a ramp terminal voltage which rises over a long time, say 100 periods, to reach an accurate steady-state. The Fortran code is an order of magnitude faster than the ATP model whose relative slowness is caused by using the MODELS language in this particular model.

The dashed lines in Fig. 8 show the no-load losses and currents calculated for the *real* voltages, but using the model parameters found for the *average* (V_{avg}) voltages. The overestimated current values at large V_{avg} clearly point out the need to enlarge the stacking factor. As shown by the solid lines in Fig. 8, the value of S_F = 0.973 can be considered acceptable. This value shall be used in the next Section where the model fitted to the LV side excitations is adjusted to inrush currents resulted from excitation of outer (HV) winding.

VI. The Model Fitting to Measured Inrush Currents

The purpose of this Section is to fit the model to the maximum residual flux in the core legs (about 0.5 pu) and to the maximum inrush current (241 A) observed in the measurements [2], [11]. There are two model parameters, Δ and K, to satisfy these criteria. It will be shown in the next subsection that the residual fluxes are independent of K, so the maximum residual flux is controlled by the air gaps in the core (Δ). It can be noted that there were no core gaps in the model [11], that led to somewhat overestimated residual flux. This case is illustrated by the upper curve λ_A in Fig. 9(b), which also shows that the model fitting can be started with Δ = 0.

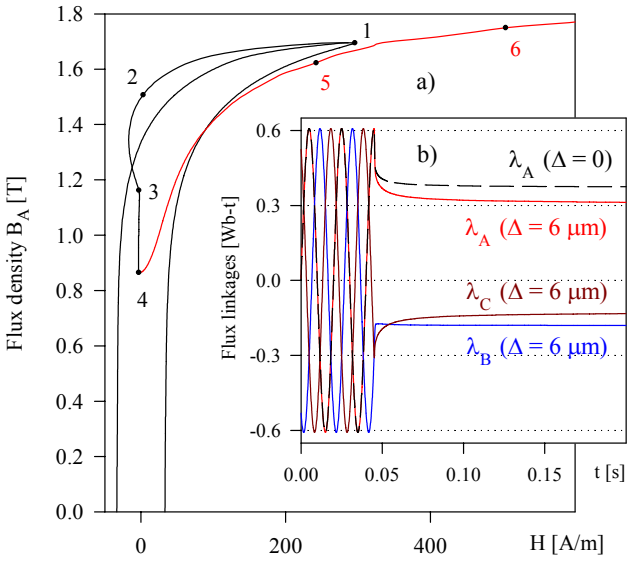

Fig. 9(a). Flux density in the leg A during the ring-down transient. Point 1 is for chopping instance, curve 1-2-3 is for fast dropping flux interval, 3-4 shows the slow dropping flux interval, 4-5-6 is for subsequent inrush current. Fig. 9(b) shows flux linkages of the windings of phases A, B, and C.

A. Ring-down and inrush modeling by means of the simplified model

As in almost all existing models, the analysis in this subsection is carried out using the *simplified* model (switches S are closed in the circuit of Fig. 4 to eliminate inductances L_0 and discard the Cauer circuit). The only elements representing the tank in this model are inductances L_{03}. In accordance with [23] and [12], L_{03} = 0.42 mH.

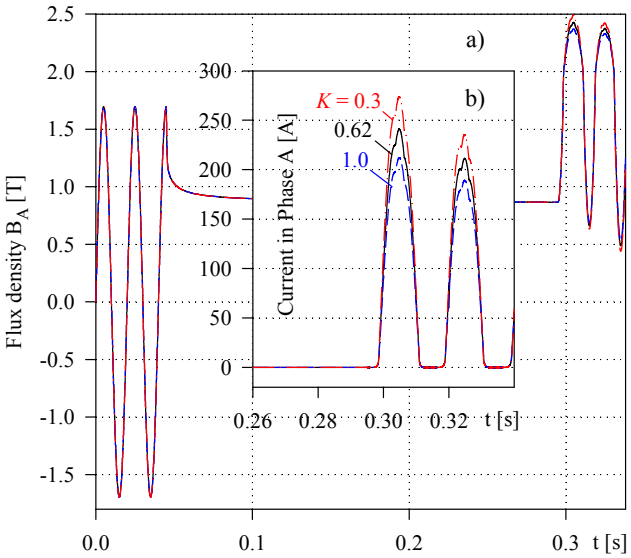

Fig. 10. Inrush current events in phase A at Δ = 6 μm.

The modeling of this subsection is illustrated by Figs. 9 and 10, in which the flux linkages during the no-current pause are independent of K.

The ring-down transients are modeled for the case when the transformer with open-circuited LV windings is also disconnected from the HV supply. Due to the auto-initialization of the model at t < 0, the modeling begins with a steady-state (see the first periods in Fig. 9(b)). At S_F = 0.973 found in the previous section, one per unit (1 pu) flux linkage of the windings is 0.6073 Wb-turns.

The currents in all three HV windings are assumed to be chopped at the instant (t_1 = 0.045 s) when flux linkage λ_A (and flux density B_A) in phase A reaches a maximum (point 1 in Fig. 9(a)). The chopping is followed by a complex transient [10], which is manifested by aperiodically decreasing fluxes in the legs, as shown in Fig. 9(b).

The first stage of the flux decrease is a fast transient governed mainly by discharge of transformer capacitances, while the prolonged process of reaching steady-state residual fluxes is caused by a slow transient governed by inductances of the model. The fast and slow stages of the ring-down are represented in Fig. 9(a) by trajectories 1-2-3 and 3-4 respectively.

As could be expected, the largest residual flux (in absolute value) is established in the leg A. The *B–H* trajectories in Fig. 9(a) were calculated for measured transformer capacitances. Similar calculations made for capacitances deviated by 50% (on either side) from the measured capacitances show no significant variation in residual performance and thus in subsequent transformer energization (it is represented by trajectory 4-5-6 in Fig. 9(a) and is considered in the next subsection).

The effect of Δ was explained in [10] by showing that increasing Δ results in the inclination of *static* hysteresis loop of the core leg that, in turn, can make the effective remanent induction much less than the true material value. It was found in numerical experiments that the required residual flux is obtained at Δ = 6 μm, see Fig. 9(b).

It is important to note that fluxes and flux densities in the legs during the no-current pause are independent of K. This can be seen in Fig. 10(a), which shows flux densities in the leg A and currents in phase A calculated for K = 0.3, 0.62, and 1.0.

For the transformer model with chosen K_{loss}, S_F, and Δ, the only fitting parameters responsible for inrush current peaks is the coefficient K.

To consider the inrush currents, the no-current pause in the scenario in Fig. 9(b) was prolonged to the instant (t_2 = 0.295 s) when the voltage in phase A crosses zero going positive. At this instant, all three windings are reconnected to the HV source simultaneously.

The influence of K can be seen in Fig. 10. The increasing of K increases the inductance L_{01}= K L_{12}, which is a component of the "air-core" incremental inductance of the leg [2]. So, the bigger K, the less the inrush current peak. For example, at Δ = 6 μm and K = 0.3, 0.62, and 1.0, maximum current peaks are 274 A, 241 A, and 212 A respectively. This means that the maximum current peak (241 A) found in the measurements is obtained at K = 0.62.

The calculation made for a longer time, shows the same inrush current decay as that in the measurements [11].

B. Inrush currents verification using transformer model with tank submodel (Cauer circuit)

According to more detailed information about the zero-sequence (ZS) impedance of the transformer, the value of Z_0 measured from the LV terminals is not constant [23]. Its dependence on the terminal voltage found in the ZS test is shown by dots in Fig. 11.

At this point we can recall that the simplified transformer model with any constant L_{03} (any reluctance R_{03} in Fig. 3) does not reproduce the fact that the walls of the tank form an electrically conducting loop, which plays a role of a short-circuited winding enclosing all three wound legs ([22], p. 109). The current of this virtual winding is the input current of the Cauer circuit in Fig. 4, which yields practically the same results at 14 and 24 π-cells.

The fitting parameters of the model with Cauer circuit are the linear inductances L_{03} and L_0. The thickness and resistivity of the tank steel were taken equal to 4 mm and 0.16 μΩ·m respectively. The height of the modeled central belt of the tank walls was set equal to the length of the core legs. Then using the fitting technique in [16], the measured Z_0 values in Fig. 11 are approximated sufficiently well with L_{03} = 0.318 mH and L_0 = 0.273 mH. The calculated total losses of the fitted model in the ZS test (they are shown in the inset of Fig. 11) are in a good correspondence with the measured losses.

To illustrate the properties of the model, the Z_0(V) curve was also predicted for the HV side as if the HV neutral is accessible. In accordance with [24], the predicted curve (c) lies lower than the LV fitted curve (b) by approximately 4% that is close to the short-circuit impedance of the transformer.

The maximum inrush current calculated with the full model at Δ = 6 μm and K = 0.62 is 234 A that is only 3 percent less than that (241 A) found with the simplified model. So the influence of the tank representation is negligible in the regime considered.

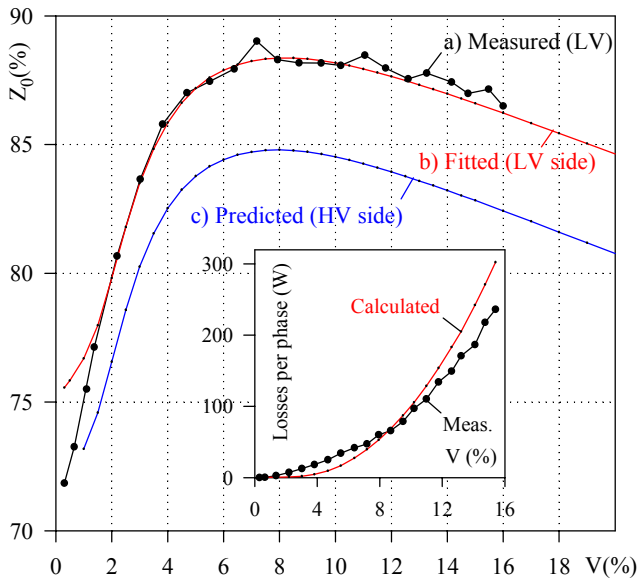

Fig. 11. Impedances Z_0 (measured from LV side) and Z_0 values (for LV and HV sides) calculated using transformer model. The measured [23] and calculated losses are shown in the inset.

VII. Magnetization versus Terminal Loops

In accordance with [3], the DHM inductors in Fig. 4 build transient curves $H(B)$, which are individual for each core branch (legs and yokes). These curves are then scaled into *magnetization* curves (loops) λ–i using the lengths and cross sections of the branches [2].

It is worth remarking that the "regular" *magnetization* λ–i loop of any *leg* differs substantially from the *terminal* λ–i loop of the corresponding phase. The reason is that the *magnetization* current is mainly determined by the flux in the own leg, whereas the current in a phase winding depends on the fluxes and thus magnetic fields in other core branches, as explained in Section 2.5.1 of [22]. In Fig. 12 this difference is illustrated for the central leg B of the core at V_{avg} = 96.67%.

The terminal loops are also different for different phases (see, for example, Fig. 1 or the "hysteresis loops" measured in [4] and [25]). This illustrates the asymmetry observed during no-load measurements on three-leg transformers [26]. A pronounced manifestation of the asymmetry is the *negative* no-load loss sometimes measured in one of the phases [26]. From a hysteretic perspective, the negative "phase loss" can be explained by an unnatural *clockwise* λ–i terminal loop of the phase, which is discovered even in a linearized topological model excited by a symmetrical three-phase voltage [27].

The case represented in Fig. 12 can be considered further by recalling that the terminal loop (it is also shown in the inset) was calculated using the "real" phase voltages of all three phases, which are Fourier series with 21 harmonics and are indistinguishable from the actual voltages. The closeness of the just-mentioned V_{avg} shows that the real terminal voltages are close, in this case, to sinusoidal, see Fig. 2.

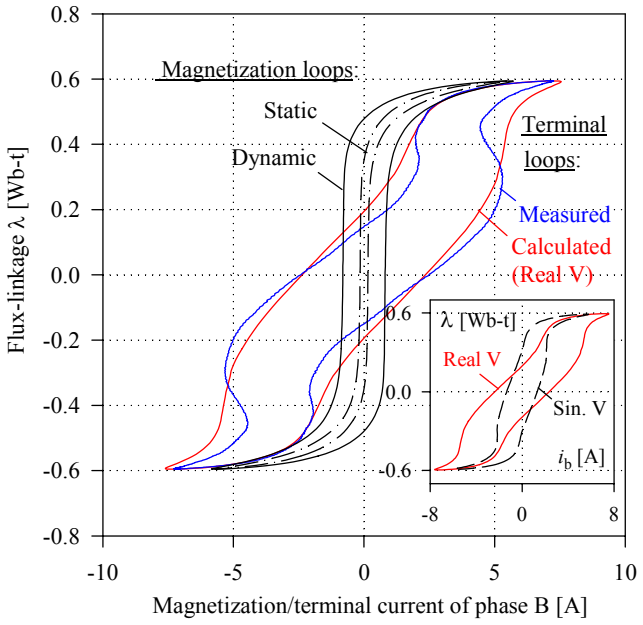

Fig. 12 Magnetization loops of the leg B and terminal loops for phase B.

It is remarkable that the terminal loop(s) calculated for the ideally sinusoidal symmetrical voltages (see loop Sin. V in the inset of Fig. 12) is quite different from the loop Real V calculated for the "almost-sinusoidal" voltage V_{avg}. The reason for this difference is somewhat different voltages of phases A (96.56%), B (97.42%), and C (96.03%). The mentioned V_{avg} = 96.67% is the mean of these values. It is also remarkable that *magnetization* λ–*i* loops of all three legs are very close. This shows that even minimal changes in the voltage waveform and a small difference between phase voltages may result in substantial changes of the terminal loops, which can take "anomalous" shapes.

It is difficult to expect that all three terminal loops will be predicted accurately. The difference between the calculated and measured loops for terminals A and C (Fig. 13) is bigger than that in Fig. 12. Nevertheless, the calculated loops in Fig. 12 and 13 show the same tendency in their area as that observed in the measurements, see Fig. 1.

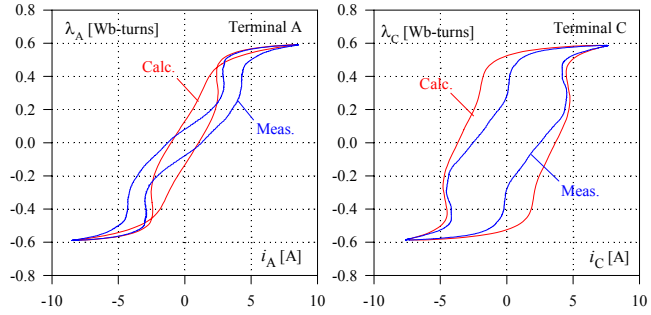

Fig. 13. Magnetization and terminal hysteresis loops for phases A and C.

The difference between the loops in Fig. 13 may be caused by the fact explained in section 2.5.1 of [22]: "The excitation current and power drawn by each phase winding are *not* the actual current and power required by the corresponding magnetic sections of the core. The current drawn by each phase winding is determined by the combination of requirements of all the three core branches." It should be also remembered that the measured no-load currents and hence the terminal loops depend on previous work of the transformer (residual fluxes) and can be different in different measurements. So, in general, the terminal loops can hardly be used directly for accurate fitting of transformer parameters.

VIII. Model Fitting with Unknown Design Parameters

The model adjustments above were carried out using the *known* number of turns (N_1 = 21), the length of the leg (L_{leg} = 0.670 m) and its geometrical cross section (S_{leg} = 0.017528 m^2). This information is proprietary and is seldom available to engineers involved in modeling and analysis. In this case, the model with the *known* SC parameters can be fitted to the OC test data by finding a minimum of the cost function

$$F(X) = W\sum_{k=1}^{N}[1 - P_c(k)/P_m(k)]^2 + (1-W)\sum_{k=1}^{N}[1 - I_c(k)/I_m(k)]^2 . \quad (4)$$

In (4), the calculated no-load losses P_c and currents I_c are compared to those (P_m and I_m) measured at a number N of terminal voltages. The weight W controls the relative cost of discrepancies in losses and currents individually. In the version described in this paper, the vector X consists of three components. To be consistent with results of the "manual" fitting in Section V, the first two components of X are the stacking factor S_F of the core and the loss coefficient K_{loss}. The third component of X is the length of the leg, L_{leg}.

Function (4) can be minimized using a method, which does not require gradients. The simplex search algorithm of Nelder-Mead was used in a dedicated Fortran program in which the losses and currents in (4) are calculated by means of the magnetic circuit in Fig. 4 with open switches *S*. It was found acceptable to make auto-initialization of the Fortran model taking into account only the fluxes in the core. Then a steady state in the model with off-core fluxes is established during several integration steps of the first period, and the values of P_c and I_c are calculated over the second period.

The loss (in watts) in a core branch (with the cross section *S* and the length *l*) is determined by its λ–*i* dynamic loop. The flux linkage λ and the (branch) current *i* are expressed as

$$\lambda = B \cdot (N_1 S) \quad (5)$$

and

$$i = \frac{l}{N_1} \cdot H \quad (6)$$

where N_1 is number of turns in the excited winding.

So, a *B*–*H* curve of the chosen steel is converted into a λ–*i* curve of the core branch using only *two* parameters, namely the product $N_1 S$ and the ratio l / N_1. As these two parameters involve the *three* physical quantities (*S*, *l*, and N_1), one of them can be chosen *arbitrarily*. To avoid the difficulties of partially integer-valued optimization, it is convenient to fix the number of turns N_1, which occurs in both (5) and (6). This

means that we can use an *arbitrary* N_1 when minimizing (4), where S and l (together with K_{loss}) are variable parameters. For any other turn number, N_{1new}, the found values of S and l are recalculated into $S_{new} = S(N_1 / N_{1new})$ and $l_{new} = l(N_{1new} / N_1)$.

At arbitrarily chosen N_1, the initial value of the leg cross section is estimated by taking into account the typical flux density in the leg, B_m, which can be set between 1.6 and 1.7 T at the rated voltage V_{rated}. Using this initial (base) flux density, $B_{m,base}$, the initial (base) value S_{base} is calculated (at frequency f) using the relationship following from the well-known voltage equation of transformer:

$$S_{base} = \frac{V_{rated}}{4.44 f \cdot N_1 \cdot B_{m,base}}. \quad (7)$$

Then the variable cross section S_{leg} of the leg is calculated as the product $S_F \times S_{base}$.

The program developed also allows one to extend vector X by adding the length of the yoke (L_{yoke}) and its cross section (S_{yoke}). However, the calculations in this paper are made at *fixed* ratios L_{yoke} / L_{leg} (=0.8657) and S_{yoke} / S_{leg} (=1.13) taken for definiteness from the design data of the considered 300 kVA transformer.

To validate the method, the procedure was initially tested at $N_1 = 21$, which is the actual turn number of the LV winding. At fixed $\Delta = 6$ μm and $K = 0.62$ found in Section VI-A, the minimum of (4), found at $W = 0.5$, is obtained at:

$$S_F = 0.9603,\ K_{loss} = 1.3342,\ L_{leg} = 0.6744 \text{ m}. \quad (8)$$

The value of L_{leg} in (8) is close to the actual one (0.670 m) used in the previous sections. The losses and currents calculated for the components in (8) are represented in Fig. 14.

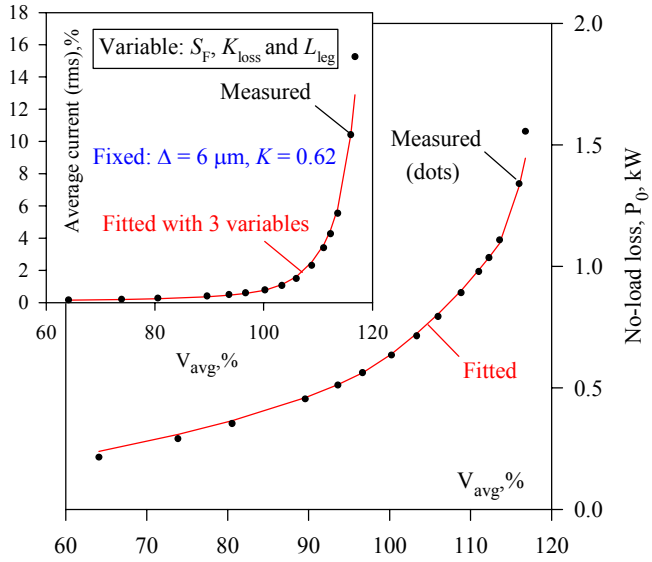

Fig. 14. No-load losses and currents calculated by minimizing (4).

To verify the code, the minimization of (4) can be repeated using another fixed turn number N_1, but keeping the same ratios L_{yoke} / L_{leg} and S_{yoke} / S_{leg}. For example, at $N_1 = 210$ (taken instead of $N_1 = 21$), we obtain the same S_F and K_{loss} as in (8), while the value of L_{leg} is exactly ten times larger, as it should be.

It is clear that the leg length of 6.744 m is obviously unnatural for the 300 kVA transformer, however this does not mean that the fitting is wrong. As the cross section areas of the core branches becomes ten times smaller at $N_1 = 210$, the core keeps its volume, flux densities, and the losses in legs and yokes. So the total no-load losses and currents keep the values represented in Fig. 14. The models fitted at $N_1 = 210$ and $N_1 = 21$ are also equivalent in any other their aspects, e.g. for inrush currents. This is because the off-core inductances and the winding resistances are held fixed and do not change when changing the core geometry. This illustrates the principal difference between the model fitting and the transformer design optimization.

IX. Conclusion

This paper outlines a method for modeling transformers using catalog data, which is often the only available information about the assumed core material. We have developed two independent versions of a topological model of the core-type three-phase transformer. One is a dedicated Fortran program written for magnetic quantities, the other is a duality-derived equivalent circuit. Both the model versions are based on a dynamic hysteresis model, which reproduces the sharp increase in core loss at high flux densities.

We show that an effective way to fit the transformer model to open-circuit test results at high voltages is to vary the core stacking factor S_F and the loss coefficient K_{loss} of the DHM inductors. We find that the residual fluxes in the transformer legs and thus the subsequent inrush currents are controlled by the air gaps Δ at the core joints. The subsequent current peaks are sensitive to the coefficient K, which determines the reluctance (inductance) of the air channel between the innermost winding and the core.

When using catalog saturation-curve data, we avoid the notions of the magnetization inductance and the incremental saturation inductance. By operating with S_F, Δ, K_{loss}, and K directly and proceeding in a physically clear manner, the transformer model can be closely fitted to open-circuit test data by simple iterative calculations.

An optimization model fitting of a transformer with unknown design parameters is proposed.

We have observed that the *terminal* λ–i loops can differ substantially from the magnetization hysteresis loops of the core legs.

When modeling inrush currents, we have found it acceptable to use the simplified transformer model, in which the zero sequence flux paths are represented by linear inductances as is commonly made in the existing models [5], [6], [11]. The influence of the tank under other operating conditions will be explored elsewhere.

X. References

[1] C. M. Arturi, "Transient simulation of a three phase five limb step-up transformer following an out-of-phase synchronization," *IEEE Trans. Power Del.*, vol. 6, no. 1, pp. 196–207, Jan. 1991.

[2] N. Chiesa, "Power transformer modeling for inrush current calculation," Doctoral theses, NTNU, 2010.

[3] S. E. Zirka, Y. I. Moroz, N. Chiesa, R. G. Harrison, and H. Kr. Hoidalen, "Implementation of inverse hysteresis model into EMTP – Part II: Dynamic model," *IEEE Trans. Power Del*., vol. 30, no. 5, pp. 2233-3241, Oct. 2015.

[4] P. S. Moses, M. A. S. Masoum, and H. A. Toliyat, "Dynamic modeling of three-phase asymmetric power transformers with magnetic hysteresis: No-load and inrush conditions," *IEEE Trans. Energy Conversion*, vol. 25, no. 4, Dec. 2010, pp. 1040-1047.

[5] X. Chen and S. S. Venkata, "A three-phase three-winding core-type transformer model for low-frequency transient studies," *IEEE Trans. Power Del*., vol. 12, no. 2, pp. 775–782, Apr. 1997.

[6] B. A. Mork, F. Gonzalez, D. Ishchenko, D. L. Stuehm, and J. Mitra "Hybrid transformer model for transient simulation—Part I: Development and parameters," *IEEE Trans. Power Del.*, vol. 22, no. 1, pp. 248-255, Jan. 2007.

[7] B. A. Mork, F. Gonzalez, D. Ishchenko, D. L. Stuehm, and J. Mitra "Hybrid transformer model for transient simulation—Part II: Laboratory measurements and benchmarking," *IEEE Trans. Power Del.*, vol. 22, no. 1, pp. 256-262, Jan. 2007.

[8] A. J. Moses, "Prediction of core losses of three phase transformers from estimation of the components contributing to the building factor," *J. Magn. Magn. Mater*., vol. 254–255, pp. 615–617, Jan. 2003.

[9] E. F. Fuchs and Y. You, "Measurement of λ–i characteristics of asymmetric three-phase transformers and their applications," *IEEE Trans. Power Del.*, vol. 17, no. 4, pp. 983-990, Oct. 2002.

[10] S. E. Zirka, Y. I. Moroz, C. M. Arturi, N. Chiesa, and H. K. Høidalen, "Topology-correct reversible transformer model," *IEEE Trans. Power Del*., vol. 27, no. 4, pp. 2037–2045, Oct. 2012.

[11] N. Chiesa, B. A. Mork, and H. Kr. Høidalen, "Transformer model for inrush current calculations: Simulations, measurements and sensitivity analysis", *IEEE Trans. Power Del*., vol. 4, pp. 2599-2608, Oct. 2010.

[12] H. Kr. Høidalen, A. Lotfi, S. E. Zirka, Y. I. Moroz, N. Chiesa, and B. A. Mork, "Benchmarking of hysteretic elements in topologically correct transformer model," in Proc. 2015 Int. Conf. Power Syst. Transients, pp. 15-18.

[13] IEEE standard test code for liquid-immersed distribution, power, and regulating transformers, IEEE Std C57.12.90-1999.

[14] IEC 60076-1 International Standard – Power transformers. 2000.

[15] R. Allcock, S. Holland, and L. Haydock, "Calculation of zero phase sequence impedance for power transformers using numerical methods," *IEEE Trans. Magn*., vol. 31, no. 3, May 1995, p. 2049.

[16] S. E. Zirka, Y. I. Moroz, and C. M. Arturi, "Accounting for the influence of the tank walls in the zero-sequence topological model of a three-phase, three-limb transformer," *IEEE Trans. Power Del.,* vol. 29, no. 5, pp. 2172–2179, Oct. 2014.

[17] S. E. Zirka, Y. I. Moroz, N. Chiesa, R. G. Harrison, and H. Kr. Hoidalen, "Implementation of inverse hysteresis model into EMTP – Part I: Static model," *IEEE Trans. Power Del*., vol. 30, no. 5, pp. 2224-2232, Oct. 2015.

[18] S. E. Zirka, Y. I. Moroz, P. Marketos, A. J. Moses, D. C. Jiles, and T. Matsuo, "Generalization of the classical method for calculating dynamic hysteresis loops in grain-oriented electrical steels," *IEEE Trans. Magn*., vol. 44, no. 9, pp. 2113–2126, Sep. 2008.

[19] Y. I. Moroz and S. E. Zirka, Inverse models of magnetic hysteresis, Apr. 9, 2014. [Online]. Available: https://sites.google.com/site/inversehysteresismodel.

[20] R. M. Bozorth, *Ferromagnetism*, Hoboken, New Jersey: John Wiley& Sons Inc., 2003.

[21] F. Fiorillo, L. R. Dupré, C. Appino, and A. M. Rietto, "Comprehensive model of magnetization curve, hysteresis loops, and losses in any direction in grain-oriented Fe–Si," *IEEE Trans. Magn*., vol. 38, no. 3, pp. 1467–1476, May, 2002.

[22] S. V. Kulkarni and S. A. Khaparde, *Transformer Engineering: Design and Practice*. New York: Marcel Dekker, 2004.

[23] D. Negri and M. Gotti, "Transformer model benchmarking," Master thesis, Politecnico di Milano, Milan, Italy, 2007.

[24] C. M. Arturi, "Zero-sequence behavior of three-limbs core two-windings three-phase transformers", *L'energia elettrica*, no. 1, pp. 1-10, 1987 (in Italian).

[25] F. Marketos, D. Marnay, and T. Ngnegueu, "Experimental and numerical investigation of flux density distribution in the individual packets of a 100 kVA transformer core," *IEEE Trans. Magn*., vol. 48, no. 4, pp. 1677–1680, Apr., 2012.

[26] R. Escarela-Perez, S. V. Kulkarni, N. K. Kodela, and J. C. Olivares-Galvan, "Asymmetry during load-loss measurement of three-phase three-limb transformers," *IEEE Trans. Power Del.,* vol. 22, no. 3, pp. 1566–1574, Jul. 2007.

[27] N. Chiesa, private communication, December 2015.

Sergey E. Zirka received the Ph.D. and D.Sc. degrees in electrical engineering from the Institute of Electrodynamics, Kiev, Ukraine, in 1977 and 1992 respectively.

Since 1972, he has been with the Department of Physics and Technology, Dnipro National University, Dnipro, Ukraine, where he has been a Professor since 1992. His research interests include the modeling of magnetization processes in electrical steels and transients in transformers of different types.

Yuriy I. Moroz received the Ph.D. degree in theoretical electrical engineering from the Institute of Modeling Problems in Energetics, the Ukrainian Academy of Sciences, Kiev, Ukraine, in 1991.

Currently, he is an Associate Professor in the Department of Physics and Technology, Dnipro National University, Dnipro, Ukraine. His research interests include the modeling of magnetization processes in electrical steels and transients in transformers of different types.

Hans Kr. Høidalen (M'05–SM'14) received the M.Sc. and Ph.D. degrees in electrical engineering from the Norwegian University of Science and Technology (NTNU), Trondheim, Norway, in 1990 and 1998, respectively.

Currently, he is a Professor at the NTNU with a special interest in power system transients as well as electrical stress calculations and modeling. In recent years, the focus has been on transformer analysis and power system protection. He is the developer of the preprocessor to EMTP-ATP called ATPDraw.

Nicola Chiesa received the M.Sc. degree in electrical engineering from Politecnico di Milano, Milano, Italy, in 2005 and the Ph.D. degree in electrical engineering from the Norwegian University of Science and Technology, Trondheim, Norway, in 2010.

From2009 to 2013, he was a Research Scientist at SINTEF Energy Research, Trondheim, Norway, with a special interest in power transformers, transient simulations, power electronics, and energy-storage systems. In 2013, he joined Statoil, Trondheim, Norway, in the research-and-development department with a special interest in subsea power systems for oil and gas applications.

Abbas Lotfi received the B.Sc. and M.Sc. degrees in Electrical Engineering from state university of Zandjan, Iran in 2004 and 2007 respectively. During 2007-2009, he worked in Iran Transfo company as R&D engineer in Zandjan.

From 2009 to 2010, he joint to R&D department of Pars Switch Co. as research engineer in Zandjan. He has been PhD student and held a fellowship for doctoral studies in Norwegian University of Science and Technology since 2012. His main research interests are transformer design and modeling, power system transient and modeling of submarine HV cables.

Cesare M. Arturi (M'87) received the electrical engineering degree from the Politecnico di Milano, Milan, Italy, in 1975.

Currently, he is Full Professor in the Department of Electronics, Information Science and Bioengineering, Politecnico di Milano. His main fields of research activity include the modeling of parametric energy conversion devices, power transformers, and the thermodynamic approach to the electromagnetic conversion devices.